Available online at www.sciencedirect.com
SCIENCE DIRECT®
Journal of volcanology and geothermal research
ELSEVIER
Journal of Volcanology and Geothermal Research 131 (2004) 1–18
www.elsevier.com/locate/jvolgeores

Comagmatic granophyre and dacite from Karymsky volcanic center, Kamchatka: experimental constraints for magma storage conditions

Pavel Izbekov *, James E. Gardner, John C. Eichelberger

Alaska Volcano Observatory, Geophysical Institute, University of Alaska, Fairbanks, AK 99775-7320, USA

Received 9 October 2002; accepted 11 August 2003

Abstract

Despite a ~30 000 years difference in age, two caldera-forming eruptions at Karymsky volcanic center, Kamchatka – Karymsky (7900 yr BP) and Academy Nauk (ca. 40 000 yr BP) – produced two-pyroxene dacites with the same composition and mineralogy. Granophyric xenoliths of the identical whole-rock chemistry were found in basalts erupted within Academy Nauk caldera in 1996. Unlike the dacites, however, the granophyres are holocrystalline and contain biotite and amphibole. Large amphibole phenocrysts contain rare inclusions of clinopyroxenes, which compositionally overlap with clinopyroxenes in the dacites. The Al content of the amphibole suggests it grew at a pressure of about 100 MPa. Results of hydrothermal experiments and petrologic observations indicate that Academy Nauk and Karymsky dacites were last equilibrated at 883 ± 19°C, 100 ± 15 MPa and 871 ± 19°C, 85 ± 18 MPa, respectively, both at water-saturated conditions. The mineral assemblage of granophyre is reproduced by isobaric crystallization of the dacite at 100 MPa, implying that the granophyres were sampled from the crystallized silicic reservoir that produced the caldera-forming eruption of Academy Nauk. Similar chemical compositions of Karymsky and Academy Nauk dacites indicate that both were derived from the same crustal-level source. The eruptive history of the calderas can best be explained by two 10–12-km^3 dacitic batches that detached from a parental body situated in the lower crust, then ascended to 3–4 km depth, re-equilibrated, and erupted.

Keywords: dacite; granophyre; calderas; Kamchatka Peninsula; experimental studies; petrology

1. Introduction

Nested or closely located calderas are common features of volcanic arcs, e.g., Taupo, New Zealand (Sutton et al., 1995), Aso, Japan (Lipman, 1967) and Ksudach, Russia (Volynets et al., 1999). They form as the result of repeated voluminous eruptions of silicic magmas at a single volcanic center. Different models have been proposed to explain the recurrence of silicic volcanism, ranging from those in which the magmas are fed from a single long-lived reservoir to those in which they are generated by fast, repetitive partial melting (Huppert and Sparks, 1988; Sparks et al., 1990). Volumes, depths, residence times, and histories of replenishments of individual magma

* Corresponding author.
E-mail address: pavel@gi.alaska.edu (P. Izbekov).

0377-0273/03/$ – see front matter © 2003 Elsevier B.V. All rights reserved.
doi:10.1016/S0377-0273(03)00312-3

systems linked to caldera-forming eruptions significantly vary from one volcanic center to another, and thus each case must be considered on an individual basis.

This paper presents results of a petrologic and phase-equilibrium experimental studies, which provide a basis for understanding the magma system at Karymsky and Academy Nauk (AN), neighboring eruptive centers of the eastern volcanic front of Kamchatka. An important finding is that the dacites of the last two caldera-forming eruptions are virtually identical in composition, despite being separated in time by ~30 000 years. In addition, granophyric inclusions in basalt erupted in 1996 match the dacites in composition. These findings raise two questions concerning the system. First, were the granophyric xenoliths sampled from the crystallized silicic reservoir that produced either of the calderas? And second, what magmatic process could repeatedly produce dacitic magma of exactly the same composition over a ~30 000-year period?

2. Geological background

Karymsky volcanic center is located in the middle of the eastern volcanic front of Kamchatka,

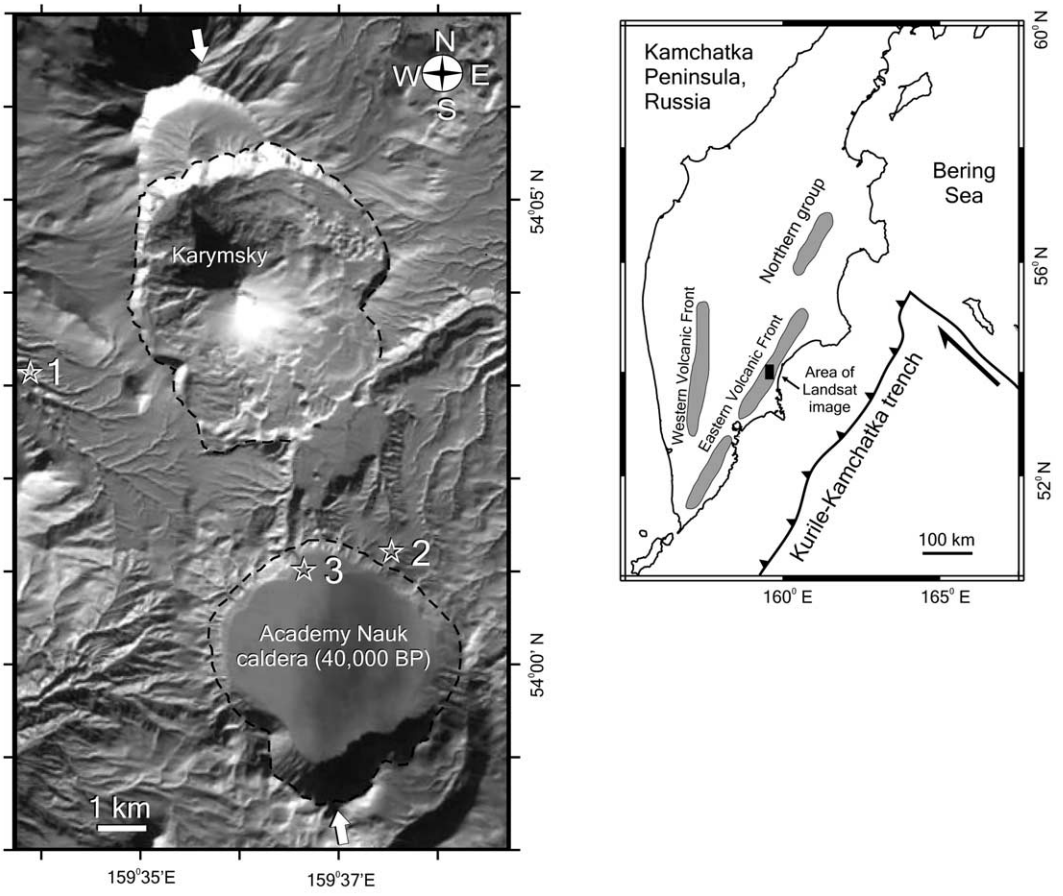

Fig. 1. Landsat-4 image of Karymsky volcano and AN caldera centered 9 km apart. Arrows indicate a longitudinally oriented fault zone between the volcanoes. Stars show the sites of sample collection: 1 = Karymsky dacites (99IPE4), 2 = AN dacites (99IPE6) and 3 = granophyre xenoliths from basalts erupted in 1996 (97IPE7). Caldera rims are delineated with dotted lines. The position of the volcanoes within the volcanic arc of Kamchatka is shown on the inset.

approximately 120 km above the westward-dipping subducting slab of the Pacific plate (Fig. 1). The center consists of several volcanoes and calderas, three of which – Karymsky, Maly Semiachek, and AN – erupted in the 20th century. Volcanic activity at Karymsky volcanic center started at about 2 Ma. Since that time the volumetric eruption rate has decreased significantly, whereas magma compositions progressed from strongly bimodal to dominantly andesitic, although the overall range of compositions remained the same – from basalts to rhyolites (Masurenkov, 1980).

AN and Karymsky are two adjacent 5-km-diameter calderas, situated along a longitudinally oriented fault zone (Fig. 1). AN caldera is the youngest of two nested calderas formed in a succession of two alternating cone-building and caldera-forming events in the southern part of the studied area. The age of the caldera is $40\,000 \pm 10\,000$ yr BP, based on the fission-track study of obsidian xenoliths from the basal plinian fall layer (Masurenkov, 1980). Following the last caldera-forming event, eruptive activity within the caldera has been restricted to phreatomagmatic basaltic eruptions, the most recent of which occurred in 1996 (Belousov and Belousova, 2001; Braitseva, 1998; Izbekov et al., 2002). Basalts, which erupted in the northern part of AN caldera in 1996, contained xenoliths of silicic rocks – granites, pumices, and altered tuffs – which were probably plucked from the walls of the conduit by the ascending magma. Grib (1998) suggested that some of the xenoliths, i.e., dacite–rhyolite pumices, could represent material from the silicic magma reservoir that produced the caldera-forming eruption 40 000 yr BP.

Karymsky caldera was explosively formed 7900 yr BP as the result of eruption of 5–7 km^3 of dacite with collapse of Pra-Karymsky volcano (Braitseva and Melekestsev, 1991). After a 2500-year period of quiescence, activity within the caldera resumed with the eruption of basalts, and the stratocone of modern Karymsky began to grow. The composition of erupted magma quickly changed to andesitic, and has remained almost constant for the last 500 years. Karymsky volcano, which now occupies most of the caldera, has had seven periods of intermittent eruptive activity in the 20th century (Ivanov, 1970). The last period started in January 1996, simultaneously with basaltic eruption within AN caldera, and continues at the time of writing.

3. Samples and techniques

The sample of the AN caldera-forming eruption (99IPE6) used in this study consists of pumice clasts collected from the basal plinian fall deposit (Site no. 274 of Masurenkov, 1980). The sample of the 7900 yr BP Karymsky caldera-forming eruption (99IPE4) was collected from a 3-m-thick layer of tightly packed pumice blocks, located in the middle of pyroclastic flow deposit (KPM unit of Braitseva and Melekestsev, 1991). Five samples of granophyric xenoliths, including 97IPE7, were collected from the top of the lapilli–ash tuff ring formed by the 1996 basaltic eruption, located in the northern part of AN caldera. In this study we used only the interiors of large, 0.3–0.4-m granophyric blocks, which show no signs of reaction with the host basalt.

3.1. Experimental techniques

Natural dacite pumices were crushed to a fine powder in order to be used as starting materials for hydrothermal experiments. An experimental run consisted of either natural powder or pre-run material plus water, contained in $Ag_{70}Pd_{30}$ tubes. The tubes (2 or 5 mm in diameter) were welded with an oxy-acetylene torch at one end. Between 30 and 450 mg of sample plus a weighed amount of deionized water were added. The amount of water added was sufficient to ensure that excess water vapor was present in each run. Finally, the open end of the tube was welded shut. Capsules were weighed before and after welding to ensure that no water was lost.

All experiments were run in externally heated, René-style pressure vessels with nickel filler rods, and water as the pressurizing medium. Reaction between the Ni-alloy vessel, filler rod and the pressurizing water buffered oxygen fugacity of the run at an f_{O_2} of 0.5–1.0 log units above the Ni–NiO buffer curve (Geschwind and Rutherford,

1992; Gardner et al., 1995). Pressure was monitored using a pressure transducer with a precision of ±0.1 MPa. Temperature was measured using chromel–alumel thermocouples precise to ±3°C.

Two sets of experiments were conducted. The first set constrained the pre-eruptive storage conditions of AN and Karymsky dacites (Table 1). Pressures and temperatures for such experiments were chosen on the basis of estimates from compositions of hornblende and Fe–Ti oxides in our natural samples. Depending on the choice of starting material, experiments were either crystal-

Table 1
Conditions of experimental runs

Run	Starting material	*P* (MPa)	*T* (°C)	Duration (h)	Products[a]
PI-1	99IPE4	100	850	96	Pl, OPx, CPx, Op, G, V
PI-2	99IPE4	100	900	96	OPx, CPx, G, V
PI-3	PI-1	100	875	96	Pl, OPx, CPx, Op, G, V
PI-4	PI-2	100	875	96	Pl, OPx, CPx, Op, G, V
PI-5	PI-1	50	875	120	Pl, OPx, CPx, Op, G, V
PI-6	PI-2	50	875	120	Pl, OPx, CPx, Op, G, V
PI-7	PI-1	150	875	96	OPx, CPx, Op, G, V
PI-8	PI-2	150	875	96	OPx, CPx, Op, G, V
PI-9	99IPE4	100	900	120	OPx, CPx, G, V
PI-10	PI-1	75	875	120	Pl, OPx, CPx, Op, G, V
PI-11	PI-9	75	875	120	Pl, OPx, CPx, Op, G, V
PI-12	99IPE4	100	825	96	Pl, OPx, CPx, Op, G, V
PI-13	99IPE4	200	825	120	Pl, Hb, CPx, G, V
PI-14	PI-12	50	900	96	Pl, OPx, CPx, Op, G, V
PI-15	PI-2	50	900	96	Pl, OPx, CPx, Op, G, V
PI-16	PI-12	100	800	120	Pl, OPx, CPx, Op, G, V
PI-17	PI-13	200	800	96	Pl, Hb, CPx, G, V
PI-19	PI-16	100	775	96	Pl, OPx, CPx, Op, G, V
PI-20	PI-17	200	775	96	Pl, Hb, CPx, G, V
PI-21	PI-17	200	750	96	Pl, Hb, G, V
PI-22	PI-19	100	750	96	Pl, OPx, CPx, Op, G, V
PI-23	PI-22	100	725	144	Pl, OPx, CPx, Op, G, V
PI-24	PI-21	200	725	144	Pl, Hb, Bt, Q, G, V
PI-26	PI-24	200	700	96	Pl, Hb, Bt, Q, G, V
PI-27	PI-26	200	725	360	Pl, Hb, Bt, Q, G, V
PI-28	PI-12	100	725	360	Pl, OPx, CPx, Op, G, V
PI-29	99IPE4	300	725	312	Pl, Hb, Bt, Q, G, V
PI-30	99IPE4	300	700	288	Pl, Hb, Bt, Q, G, V
PI-31	PI-9	75	900	204	Pl, OPx, CPx, Op, G, V
PI-32	PI-28	75	900	204	Pl, OPx, CPx, Op, G, V
PI-33	PI-9	75	850	204	Pl, OPx, CPx, Op, G, V
PI-34	PI-28	75	850	204	Pl, OPx, CPx, Op, G, V
PI-35	PI-23	150	725	336	Pl, Hb, Bt, Q, G, V
PI-36	PI-24	150	725	336	Pl, Hb, Bt, Q, G, V
PI-37	PI-20	150	825	96	Pl, OPx, CPx, Op, G, V
PI-38	PI-9	150	825	96	Pl, OPx, CPx, Op, G, V
PI-39	PI-3	125	875	96	OPx, CPx, Op, G, V
PI-40	PI-8	125	875	96	OPx, CPx, Op, G, V
PI-43	PI-37	150	775	96	Pl, Hb, CPx, G, V
PI-44	PI-36	150	775	96	Pl, Hb, CPx, G, V
PI-45	PI-27	200	750	336	Pl, Hb, G, V
PI-46	PI-21	200	775	312	Pl, Hb, CPx, G, V

[a] Pl = plagioclase, OPx = orthopyroxene, CPx = clinopyroxene, Hb = hornblende, Bt = biotite, Q = quartz, Op = opaque mineral, G = glass, V = vapor.

lizing or melting. The crystallizing experiments used an aliquot of a previous run with lower crystal content, whereas melting experiments used an aliquot with larger crystal content. Many experiments were reversal, where two charges in separate capsules, one of which was a 'crystallizing' experiment and another a 'melting', were run side by side at the same conditions and in the same pressure vessel, thus approaching crystal–melt–vapor equilibrium from two directions. The majority of experiments were run for 96 h. Several low-temperature experiments were allowed to equilibrate for 360 h.

A second set of experiments simulated isobaric crystallization of the dacites at 100 and 200 MPa (Table 1). In these experiments, a 450-mg charge of dacite was first equilibrated at near-liquidus, water-saturated temperatures. After quenching, the sample was extracted and part of it was prepared as a polished thin section. The remaining material plus additional water was run again at the same pressure but at a lower temperature. Repeated several times, the experiments modeled sequential, step-wise crystallization of the dacite. This design allowed the runs to achieve equilibrium between the melt and outer rims of growing minerals at each stage, as well as to form larger microlites while approaching the solidus. Most experiments in the second set were run for 96 h.

3.2. Analytical methods

Whole-rock compositions (Table 2) were determined at Washington State University, using X-ray fluorescence analysis (major element oxides, Ni, Cr, V, Zr, Ga, Cu and Zn) and inductively coupled plasma mass spectrometry (rare earth elements, Ba, Th, Nb, Y, Hf, Ta, U, Pb, Rb, Cs, Sr and Sc). Analytical procedures and uncertainties are discussed in Nye et al. (1994). Modes of minerals and glass in the dacite pumices were calculated by mass balance using their whole-rock, mineral, and matrix-glass compositions. The modes in granophyres were determined by point counting (1000 points) using a petrographic microscope.

Compositions of natural and synthesized minerals and glasses were obtained using the Cameca

Table 2
Whole-rock composition of 40 000 yr BP AN dacite, 7900 yr BP Karymsky dacite and granophyre xenolith

	Sample[a]		
	99IPE6	97IPE7	99IPE4
SiO_2 [b]	69.54	70.43	69.58
Al_2O_3	15.37	14.83	15.06
TiO_2	0.493	0.47	0.526
FeO*	3.23	3.31	3.33
MnO	0.093	0.064	0.088
CaO	3.27	2.79	3.28
MgO	1.04	0.93	1.09
K_2O	2.45	2.61	2.37
Na_2O	4.4	4.46	4.56
P_2O_5	0.105	0.093	0.113
Total	100	100	100
Ni	6	7	3
Cr	5	3	5
V	63	47	65
Zr	190	206	184
Ga	14	17	15
Cu	12	12	9
Zn	47	32	44
La	12.48	12.64	12.33
Ce	27.62	27.27	26.85
Pr	3.51	3.41	3.47
Nd	15.64	14.93	15.24
Sm	4.15	4.02	4.10
Eu	1.01	1.00	0.99
Gd	4.07	3.96	4.10
Tb	0.73	0.67	0.73
Dy	4.60	4.38	4.59
Ho	0.97	0.92	0.94
Er	2.86	2.74	2.79
Tm	0.44	0.43	0.43
Yb	2.91	2.80	2.76
Lu	0.46	0.46	0.45
Ba	532	557	520
Th	2.62	2.55	2.55
Nb	3.57	3.28	3.72
Y	29.78	26.70	28.61
Hf	5.28	5.43	5.10
Ta	0.29	0.30	0.30
U	1.33	1.40	1.30
Pb	8.18	5.38	7.92
Rb	35.6	35.9	34.4
Cs	1.56	1.23	1.37
Sr	248	205	241
Sc	12.0	10.1	13.1

[a] Samples are AN dacite (99IPE6), Karymsky dacite (99IPE4) and granophyre xenolith (97IPE7).

[b] Major oxides in wt% with all Fe reported as FeO, concentrations of Ni–Zn (ppm) determined by X-ray fluorescence analysis, concentrations of La–Sc (ppm) determined by inductively coupled plasma mass spectrometry.

Table 3
Composition of minerals and matrix glass in natural samples

Sample[a]	*n*	SiO_2 [b]	Al_2O_3	TiO_2	FeO^t	CaO	MnO	MgO	K_2O	Na_2O	Cl	F	Total
Glass[c]													
99IPE4 M	7	75.62 (0.39)	12.77 (0.27)	0.21 (0.05)	1.77 (0.17)	1.44 (0.07)	n.a.	0.32 (0.03)	3.15 (0.09)	4.55 (0.25)	0.16 (0.02)	n.a.	98.50
99IPE4 I	15	75.64 (0.49)	13.05 (0.23)	0.35 (0.08)	1.55 (0.16)	1.42 (0.06)	n.a.	0.29 (0.03)	3.17 (0.18)	4.35 (0.23)	0.19 (0.03)	n.a.	96.42
99IPE6 M	7	74.31 (0.49)	13.52 (0.32)	0.20 (0.05)	1.82 (0.10)	1.68 (0.13)	n.a.	0.35 (0.03)	3.04 (0.08)	4.91 (0.17)	0.18 (0.02)	n.a.	98.36
99IPE6 I	9	75.37 (1.15)	12.78 (0.71)	0.16 (0.10)	2.16 (0.27)	1.42 (0.47)	n.a.	0.30 (0.12)	3.49 (0.42)	4.13 (0.15)	0.19 (0.02)	n.a.	95.71
Plagioclase[d]													
99IPE4, R	7	56.33 (0.38)	26.68 (0.17)	n.a.	0.45 (0.06)	8.85 (0.15)	n.a.	n.a.	0.27 (0.02)	6.33 (0.13)	n.a.	n.a.	98.91
99IPE4, C	6	56.15 (0.17)	27.29 (0.76)	n.a.	0.42 (0.05)	9.12 (0.29)	n.a.	n.a.	0.23 (0.04)	5.92 (0.43)	n.a.	n.a.	99.14
99IPE6, R	5	56.08 (0.70)	27.22 (0.62)	n.a.	0.47 (0.10)	9.41 (0.30)	n.a.	n.a.	0.24 (0.06)	5.88 (0.22)	n.a.	n.a.	99.30
99IPE6, C	8	51.95 (0.66)	29.83 (0.39)	n.a.	0.47 (0.04)	12.36 (0.45)	n.a.	n.a.	0.13 (0.02)	4.44 (0.15)	n.a.	n.a.	99.18
97IPE7 R	9	60.61 (1.19)	25.29 (0.83)	n.a.	0.27 (0.10)	5.73 (0.90)	n.a.	n.a.	0.40 (0.08)	7.53 (0.54)	n.a.	n.a.	99.83
97IPE7 C	5	58.03 (0.72)	26.93 (0.71)	n.a.	0.42 (0.06)	7.61 (0.68)	n.a.	n.a.	0.30 (0.03)	6.49 (0.39)	n.a.	n.a.	99.77
Pyroxene[e]													
99IPE4, CPx	50	53.1 (0.41)	1.04 (0.14)	0.27 (0.05)	8.91 (0.36)	21.49 (0.32)	0.5 (0.08)	14.5 (0.23)	n.a.	0.34 (0.04)	n.a.	n.a.	100.04
99IPE6, CPx	6	52 (0.75)	1.61 (0.37)	0.36 (0.11)	9.05 (0.40)	21.21 (0.20)	0.5 (0.03)	14.9 (0.32)	n.a.	0.33 (0.03)	n.a.	n.a.	99.89
97IPE7, CPx	7	52.5 (0.32)	0.87 (0.03)	0.23 (0.04)	9.6 (0.21)	21.95 (0.15)	0.5 (0.08)	14.6 (0.33)	n.a.	0.31 (0.04)	n.a.	n.a.	100.5
99IPE4, OPx	50	53.8 (0.63)	0.51 (0.14)	0.16 (0.04)	20.13 (0.53)	1.18 (0.06)	1 (0.12)	22.6 (0.28)	n.a.	0.02 (0.02)	n.a.	n.a.	99.3
99IPE6, OPx	6	52.2 (0.25)	0.66 (0.05)	0.16 (0.02)	20.04 (0.46)	1.19 (0.13)	1.1 (0.13)	23.4 (0.36)	n.a.	0.02 (0.02)	n.a.	n.a.	98.67
Hydrous minerals[f]													
97IPE7, Bt	12	39.66 (0.54)	12.87 (0.35)	4.00 (0.44)	13.07 (0.67)	0.15 (0.06)	0.27 (0.09)	15.88 (0.61)	8.33 (0.26)	0.30 (0.02)	0.30 (0.06)	0.94 (0.28)	95.79
97IPE7, Hb	8	48.42 (0.29)	6.14 (0.17)	1.48 (0.21)	14.92 (0.31)	10.89 (0.24)	0.47 (0.09)	13.73 (0.17)	0.44 (0.05)	1.72 (0.10)			98.21

Composition of magnetite-ilmenite pairs[g]

Sample	TiO_2	Al_2O_3	Cr_2O_3	Fe_2O_3	FeO	MnO	MgO	Total
99IPE4, Mt	9.25	2.00	0.08	49.56	36.71	0.65	1.69	99.94
99IPE4, Ilm	42.2	0.25	0.02	21.72	32.28	0.74	2.74	99.91
99IPE6, Mt	9.17	1.95	0.07	49.76	36.3	0.68	1.85	99.78
99IPE6, Ilm	40.4	0.26	0.02	25.12	30.86	0.61	2.7	99.93

[a] Samples are Karymsky dacite (99IPE4), AN dacite (99IPE6) and granophyre (97IPE7).

[b] The average of *n* analyses (in wt%) is given together with the standard deviation (number in parentheses). Analyses of glass are normalized to 100 wt%, however the non-normalized total is reported.

[c] M = matrix glass, I = glass inclusions in pyroxenes.

[d] R = rim, C = core.

[e] OPx = orthopyroxene, CPx = clinopyroxene.

[f] Bt = biotite, Hb = hornblende.

[g] Mt = magnetite, Ilm = ilmenite.

SX-50 electron microprobe at the University of Alaska Fairbanks (Table 3). Quantitative analysis of glasses was performed using 15 kV accelerating voltage, 10 nA beam current, and a defocused beam (~10 μm diameter). In order to minimize Na migration, the count rate of Na was scanned through time and corrected using a built-in procedure (Devine et al., 1995). The composition of minerals was determined using similar analytical conditions, but with a focused beam.

The concentration of water in melt inclusions contained in natural pyroxene phenocrysts was estimated from either electron probe analyses using the 'volatiles by difference' method (Devine et al., 1995), or Fourier transform infrared spectroscopy (FTIR) analysis completed at US Geological Survey facilities in Menlo Park, following the analytical procedures described in Lowenstern et al. (1997). Precision and accuracy of electron probe analyses of melt inclusions were monitored by repetitive measurements of a KN-18 glass standard during analytical sessions (Devine et al., 1995).

4. Petrology

4.1. 40 000 yr BP AN dacite

Dacite of the AN caldera-forming eruption is highly vesicular and consists of 79 vol% microlite-free matrix glass, 16 vol% plagioclase phenocrysts, 3 vol% orthopyroxene, 1 vol% clinopyroxene, and 1 vol% magnetite ± ilmenite and apatite (Fig. 3a). Matrix glass is rhyolitic (74.31 ± 0.49 wt% of SiO_2) and does not vary among pumice clasts by more than analytical uncertainty (Table 3).

Plagioclase phenocrysts are euhedral, and contain a fine, 3–10-μm-scale oscillatory zoning superimposed on a dominant normal trend. Despite variations in their interior compositions (An_{48-63}), all plagioclases have rims of the same composition ($An_{47\pm1}$; average of five grains). Phenocrysts of ortho- and clinopyroxenes are euhedral, unzoned, and contain abundant inclusions of glass and magnetite. Magnetite phenocrysts are ubiquitous, whereas ilmenites are rare. In order to analyze ilmenites, several pumices were crushed and a hand magnet was used to make a magnetic concentrate. One magnetite–ilmenite pair and several euhedral grains of ilmenite in contact with matrix glass were found. The compositions of magnetite and ilmenite in the pair are homogeneous, uniform, and in equilibrium according to their Mg and Mn contents (Bacon and Hirschmann, 1988). The individual ilmenite grains compositionally overlap that of the ilmenite connected to the magnetite.

Nine 20–40-μm vesicle-free glass inclusions in pyroxenes were analyzed by electron microprobe. When compared on an anhydrous basis, their compositions match that of the matrix glass. The deficit in totals of glass-inclusion analyses ranges from 3.8 to 4.9 wt%, and averages 4.3 ± 0.4 wt%.

4.2. 7900 yr BP Karymsky dacite

The whole-rock composition of the dacite pumice of Karymsky caldera-forming eruption is the same as that of AN dacite (Table 2; Fig. 2). Karymsky dacite consists of 74 vol% highly vesicular, microlite-free rhyolitic glass, 20 vol% plagioclase phenocrysts, 2 vol% clinopyroxene, 2 vol% orthopyroxene, and 2 vol% magnetite ± ilmenite and apatite (Fig. 3b). The matrix glass is more silicic in composition (75.62 ± 0.39 wt%) than in the AN dacite (Table 3).

Plagioclase phenocrysts are euhedral, and show a fine oscillatory zoning superimposed on normal zoning, similar to those in AN dacite. The composition of Karymsky plagioclase is more sodic relative to that of AN plagioclase, with cores of An_{43} to An_{50} and rims of $An_{44\pm1}$. Euhedral phenocrysts of ortho- and clinopyroxene are homogeneous, and overlap considerably with those in AN dacite (Table 3). Magnetite is abundant, whereas only three ilmenite grains surrounded by glass were found in a magnetic concentrate. Compositions of magnetite and ilmenite are uniform and in equilibrium according to their Mg and Mn contents (Bacon and Hirschmann, 1988).

Pyroxene phenocrysts contain abundant glass inclusions, whose compositions overlap with that of matrix glass, on an anhydrous basis. The deficit in totals of the glass-inclusion analyses averages 3.6 ± 1.3 wt%. Three glass inclusions were also

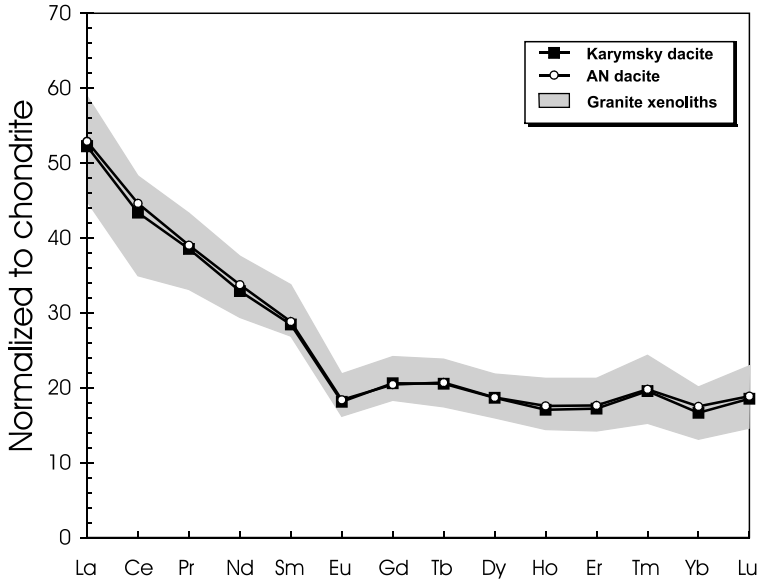

Fig. 2. Rare earth element concentrations in AN dacite, Karymsky dacite, and granophyre xenoliths (spread in values for five xenoliths) normalized to the concentrations in Orgueil chondrite (Anders and Grevesse, 1989).

analyzed by FTIR (2.52 ± 0.06, 3.67 ± 0.09, 5.07 ± 0.14 wt% of H_2O). CO_2 contents of the glass inclusions are below detection limit for FTIR (25 ppm).

4.3. Granophyric xenoliths

The whole-rock compositions of five studied granophyre xenoliths are virtually the same as compositions of the Karymsky and AN dacites (Table 3; Fig. 2). Granophyres are porphyritic (70 vol% groundmass), holo-crystalline, and the phenocryst portion consists of 41 vol% plagioclase, 20 vol% orthoclase, 28 vol% quartz, 4 vol% hornblende, 6 vol% biotite, and 1 vol% magnetite ± clinopyroxene, apatite, and zircon. The most remarkable feature of the granophyres is the micrographic texture of their groundmasses, which is formed by regular, interlocking aggregates of quartz and feldspar (Fig. 3c).

Plagioclase phenocrysts are euhedral, normally zoned, and are often in optical continuity with fringes of groundmass plagioclase radiating from their rims. Interiors of large phenocrysts range in composition from An_{27} to An_{43}. Compositions of phenocryst rims and groundmass plagioclase overlap and average $An_{29\pm5}$. Orthoclase occurs commonly as an intergrowth with quartz in the groundmass, and ranges in composition from $An_1Ab_{41}Or_{58}$ to $An_1Ab_{47}Or_{52}$.

Hornblende occurs both as euhedral, compositionally homogeneous phenocrysts and as microlites in the groundmass. The difference in composition between phenocrysts and microlites does not exceed the analytical uncertainty of the electron microprobe analysis. A few large phenocrysts of hornblende contain inclusions of clinopyroxene (Fig. 3d), the compositions of which are close to those of clinopyroxene in AN and Karymsky dacites (Table 3). Hornblende is closely associated with biotite, which has an average composition of $Annite_{31}Phlogopite_{67}Siderophyllite_2$. Magnetite abounds and often contains exsolution lamellae of ilmenite.

5. Experimental results

Because whole-rock compositions of Karymsky and AN dacites are nearly identical, phase-equilibrium experiments were performed on Karymsky dacite as a proxy for both (99IPE4; Table 2). Mineral–melt equilibria were studied over a range of water-saturated pressures from 50 to

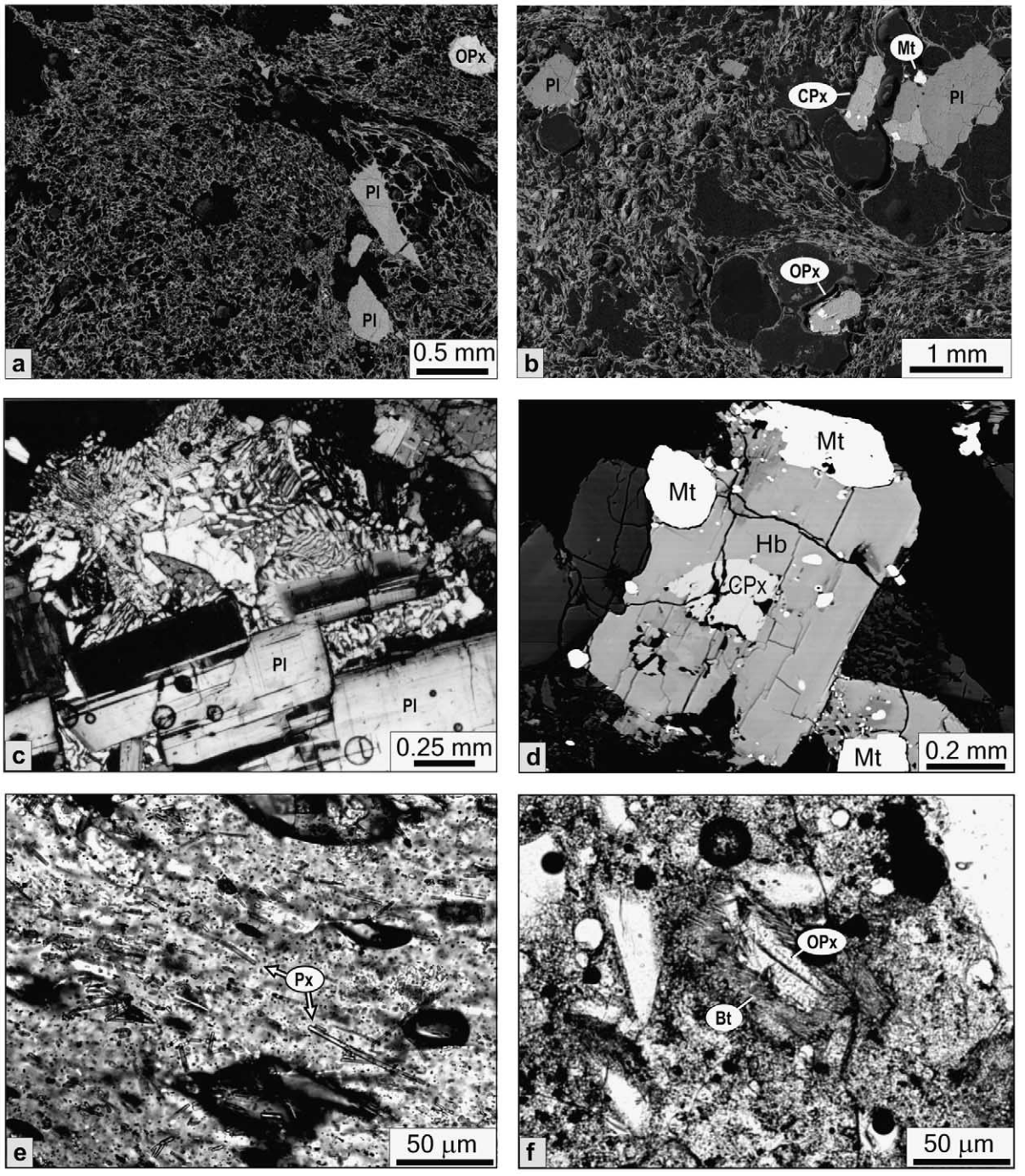

Fig. 3. Back-scattered electron images of (a) AN and (b) Karymsky dacite pumices showing phenocrysts of plagioclase (Pl), clinopyroxene (CPx), orthopyroxene (OPx), and magnetite (Mt). (c) Photomicrograph of granophyre showing 'micrographic' texture of groundmass formed by quartz–feldspar intergrowth (light is polarized). (d) Back-scattered electron image of granophyre showing a clinopyroxene inclusion inside a hornblende (Hb) phenocryst. (e) Photomicrograph of experimental run PI-37 showing euhedral microlites of pyroxenes. (f) Photomicrograph of experimental run PI-30 showing biotite (Bt) reaction rim surrounding orthopyroxene.

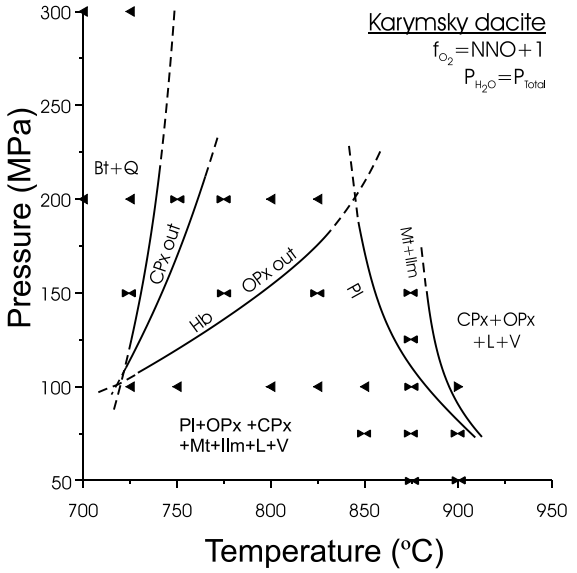

Fig. 4. Phase diagram for the Karymsky dacitic bulk composition, showing determined fields of stability of hornblende (Hb), biotite (Bt), clinopyroxene (CPx), orthopyroxene (OPx), magnetite (Mt), ilmenite (Ilm), and quartz (Q). Left-pointing arrows represent crystallization experiments; right-pointing arrows represent melting experiments.

300 MPa and temperatures from 700 to 900°C (Fig. 4). Microlites crystallized in all experiments, being most abundant at low temperatures. The presence of euhedral microlites (Fig. 3e) and overlapping compositions of melt in reversal experiments indicate that equilibrium among residual melt, outermost phenocryst rims and microlites was closely approached in all experiments, including those run for 96 h. Plagioclase microlites are usually larger than 10 μm, which allowed quantitative microprobe analysis. Other crystalline phases are usually 1–4 μm in size, limiting their analysis to qualitative EDS identification.

Pyroxenes are the first phases to crystallize at near-liquidus conditions within the investigated pressure range (Fig. 4). Lowering the temperature causes precipitation of magnetite and ilmenite, and then plagioclase. Further crystallization follows two significantly different scenarios. At pressures below 100 MPa, orthopyroxene, clinopyroxene, plagioclase, magnetite, and ilmenite crystallize simultaneously within the investigated temperature range. In contrast, isobaric cooling at pressures above 100 MPa causes an overall change from a high-temperature orthopyroxene+clinopyroxene mineral assemblage to a low-temperature hornblende+biotite assemblage. Interestingly, orthopyroxene never grew in equilibrium with hydrous minerals (Fig. 3f), similar to experimental results for the Toba Tuff (Gardner et al., 2002).

Residual melts in our experiments vary systematically in composition with pressure and temperature (Table 4). Concentrations of SiO_2 and K_2O increase, and concentrations of FeO, MgO, Al_2O_3 and CaO decrease, as temperature decreases isobarically (Fig. 5). Concentrations of SiO_2 and K_2O decrease, and concentrations of Al_2O_3 and CaO increase, as pressure increases isothermally. Concentrations of FeO and MgO in melt depend strongly on temperature, whereas their variations with pressure are not systematic.

Compositions of plagioclase microlites in our experiments vary systematically with pressure and temperature (Table 4). Plagioclase becomes progressively more sodic with decreasing temperature and pressure (Fig. 6).

6. Discussion

An intriguing finding of this study is that the caldera-forming dacites of Karymsky and AN have remarkably similar whole-rock compositions, despite their separation in time by ~30 000 years. Mineral assemblages of the dacites are also the same, although the compositions of phenocrysts and matrix glasses are conspicuously different. The granophyric xenoliths have the same whole-rock compositions as the dacites, but unlike the dacites they are holo-crystalline and contain a mineral assemblage that reflects a lower temperature of solidification.

In the following sections, the origin of the xenoliths is discussed first and then used in conjunction with glass-inclusion data to argue that the dacitic magmas were water-saturated immediately prior to their erupting. Experimental and mineral data are then used to constrain the pre-eruptive pressures and temperatures for erupted dacitic magmas. Finally, possible scenarios are discussed

Table 4
Composition of residual melt and plagioclase microlites in experimental runs

Run	*n*	SiO_2	Al_2O_3	TiO_2	FeO^t	CaO	MgO	K_2O	Na_2O	Cl	Total
Glass											
PI-1	8	75.27 (0.24)	13.21 (0.20)	0.24 (0.08)	1.67 (0.11)	1.40 (0.05)	0.27 (0.03)	3.24 (0.10)	4.48 (0.26)	0.03 (0.02)	95.91
PI-2	5	74.48 (0.32)	13.49 (0.21)	0.22 (0.07)	2.00 (0.11)	1.72 (0.11)	0.34 (0.03)	2.94 (0.11)	4.47 (0.16)	0.12 (0.01)	96.07
PI-3	15	74.94 (0.31)	13.26 (0.22)	0.25 (0.07)	1.79 (0.09)	1.62 (0.09)	0.34 (0.06)	3.12 (0.13)	4.40 (0.20)	0.08 (0.03)	96.60
PI-4	15	74.59 (0.44)	13.22 (0.16)	0.27 (0.07)	2.03 (0.11)	1.77 (0.12)	0.36 (0.04)	3.02 (0.08)	4.35 (0.32)	0.16 (0.02)	96.87
PI-5	15	76.21 (0.90)	12.54 (0.60)	0.23 (0.17)	1.71 (0.21)	1.19 (0.30)	0.18 (0.03)	3.35 (0.19)	4.32 (0.31)	0.07 (0.02)	98.22
PI-6	16	75.58 (0.72)	12.68 (0.44)	0.26 (0.10)	1.95 (0.19)	1.41 (0.26)	0.34 (0.13)	3.15 (0.12)	4.25 (0.21)	0.15 (0.02)	98.38
PI-7	13	74.44 (0.36)	13.40 (0.21)	0.25 (0.09)	2.01 (0.12)	1.84 (0.08)	0.43 (0.04)	2.92 (0.11)	4.37 (0.24)	0.12 (0.02)	95.85
PI-8	11	74.74 (0.41)	13.44 (0.29)	0.24 (0.07)	1.83 (0.11)	1.80 (0.17)	0.37 (0.04)	3.03 (0.11)	4.31 (0.23)	0.05 (0.02)	96.39
PI-10	23	75.29 (0.35)	13.26 (0.14)	0.29 (0.14)	1.66 (0.17)	1.42 (0.06)	0.27 (0.03)	3.27 (0.11)	4.29 (0.16)	0.06 (0.02)	96.23
PI-11	13	74.86 (0.26)	13.25 (0.12)	0.35 (0.14)	1.97 (0.14)	1.58 (0.09)	0.29 (0.04)	3.06 (0.12)	4.29 (0.20)	0.13 (0.03)	96.14
PI-12	20	75.35 (0.51)	13.09 (0.17)	0.42 (0.23)	1.70 (0.19)	1.42 (0.16)	0.28 (0.11)	3.21 (0.10)	4.19 (0.20)	0.15 (0.02)	94.17
PI-13	18	74.96 (0.64)	13.64 (0.35)	0.26 (0.14)	1.61 (0.14)	1.74 (0.12)	0.29 (0.05)	3.06 (0.10)	4.12 (0.19)	0.13 (0.02)	92.55
PI-14	11	76.09 (0.33)	12.26 (0.31)	0.23 (0.05)	1.95 (0.12)	1.28 (0.07)	0.24 (0.03)	3.29 (0.11)	4.31 (0.20)	0.14 (0.03)	97.70
PI-15	8	75.11 (0.42)	12.93 (0.33)	0.58 (0.11)	1.81 (0.10)	1.35 (0.08)	0.21 (0.03)	3.42 (0.12)	4.32 (0.25)	0.06 (0.03)	98.10
PI-16	8	77.08 (0.63)	12.38 (0.26)	0.36 (0.30)	1.16 (0.14)	1.05 (0.10)	0.10 (0.02)	3.55 (0.12)	4.07 (0.24)	0.13 (0.03)	94.81
PI-17	7	75.78 (0.54)	13.28 (0.26)	0.30 (0.10)	1.47 (0.11)	1.59 (0.08)	0.16 (0.02)	3.07 (0.11)	4.10 (0.34)	0.09 (0.02)	92.00
PI-20	7	75.59 (0.53)	13.41 (0.19)	0.08 (0.07)	1.22 (0.15)	1.63 (0.06)	0.12 (0.02)	3.21 (0.15)	4.56 (0.30)	0.04 (0.02)	91.74
PI-21	6	76.48 (0.58)	12.95 (0.23)	0.12 (0.07)	1.06 (0.12)	1.58 (0.05)	0.09 (0.01)	3.03 (0.11)	4.50 (0.37)	0.07 (0.04)	91.91
PI-22	7	78.81 (0.34)	11.27 (0.16)	0.12 (0.09)	0.94 (0.09)	0.72 (0.08)	0.09 (0.01)	3.81 (0.06)	4.07 (0.26)	0.06 (0.02)	95.52
PI-23	7	78.05 (0.32)	11.48 (0.30)	0.25 (0.07)	0.93 (0.11)	0.47 (0.06)	0.05 (0.02)	4.67 (0.15)	3.92 (0.29)	0.07 (0.03)	96.14
PI-24	7	77.19 (0.58)	12.63 (0.46)	0.10 (0.06)	1.06 (0.09)	0.96 (0.05)	0.06 (0.01)	3.59 (0.12)	4.22 (0.34)	0.07 (0.03)	93.76
PI-26	5	77.17 (0.68)	12.78 (0.52)	0.10 (0.05)	0.77 (0.12)	0.91 (0.18)	0.04 (0.01)	3.82 (0.23)	4.28 (0.30)	0.04 (0.03)	95.12
PI-27	7	77.09 (0.29)	13.28 (0.35)	0.08 (0.05)	0.96 (0.09)	0.96 (0.08)	0.06 (0.01)	3.48 (0.07)	3.94 (0.22)	0.05 (0.03)	94.46
PI-28	8	78.98 (0.50)	11.41 (0.43)	0.10 (0.06)	0.92 (0.28)	0.51 (0.07)	0.07 (0.05)	4.30 (0.15)	3.50 (0.19)	0.12 (0.03)	95.24
PI-29	6	77.62 (0.38)	12.96 (0.49)	0.05 (0.08)	0.73 (0.17)	1.14 (0.15)	0.08 (0.05)	3.28 (0.11)	4.00 (0.15)	0.05 (0.04)	91.02
PI-30	8	77.02 (0.88)	12.54 (0.60)	0.05 (0.06)	0.90 (0.32)	1.05 (0.29)	0.09 (0.05)	4.34 (0.41)	3.88 (0.34)	0.03 (0.02)	91.58
PI-31	7	74.62 (0.24)	13.48 (0.19)	0.23 (0.07)	2.21 (0.16)	1.70 (0.10)	0.21 (0.02)	3.01 (0.13)	4.20 (0.38)	0.09 (0.02)	97.19
PI-32	7	74.66 (0.37)	12.96 (0.27)	0.21 (0.06)	2.16 (0.13)	1.84 (0.05)	0.24 (0.02)	3.27 (0.08)	4.30 (0.40)	0.12 (0.02)	96.19
PI-33	6	75.92 (0.44)	12.57 (0.13)	0.20 (0.05)	1.74 (0.13)	1.28 (0.06)	0.14 (0.02)	3.40 (0.13)	4.41 (0.34)	0.16 (0.03)	97.06
PI-34	5	76.11 (0.60)	12.80 (0.49)	0.17 (0.05)	1.68 (0.13)	1.26 (0.13)	0.14 (0.02)	3.29 (0.17)	4.22 (0.22)	0.15 (0.02)	97.82
PI-35	6	76.84 (0.29)	12.93 (0.35)	0.23 (0.19)	0.93 (0.19)	0.87 (0.11)	0.09 (0.05)	4.13 (0.18)	3.74 (0.13)	0.12 (0.03)	93.93
PI-36	10	78.48 (0.49)	12.07 (0.14)	0.17 (0.16)	0.74 (0.19)	0.74 (0.06)	0.06 (0.03)	3.78 (0.15)	3.86 (0.25)	0.01 (0.01)	93.65
Plagioclase											
PI-1	4	57.62 (0.76)	26.65 (0.44)	n.a.	0.51 (0.07)	8.72 (0.31)	n.a.	0.31 (0.08)	6.22 (0.13)	n.a.	99.40
PI-3	3	57.69 (0.54)	26.35 (0.41)	n.a.	0.52 (0.09)	8.58 (0.17)	n.a.	0.31 (0.00)	6.27 (0.02)	n.a.	99.73
PI-4	2	56.81 (1.01)	27.64 (0.70)	n.a.	0.56 (0.16)	9.51 (0.85)	n.a.	0.27 (0.03)	5.81 (0.33)	n.a.	100.59
PI-5	2	59.71 (0.54)	25.01 (0.50)	n.a.	0.52 (0.11)	6.75 (0.04)	n.a.	0.43 (0.00)	7.21 (0.07)	n.a.	99.63
PI-6	3	59.69 (0.38)	25.12 (0.51)	n.a.	0.46 (0.14)	6.83 (0.25)	n.a.	0.46 (0.08)	6.91 (0.14)	n.a.	99.46
PI-7	3	56.53 (0.32)	26.81 (0.13)	n.a.	0.50 (0.02)	8.81 (0.03)	n.a.	0.27 (0.04)	6.07 (0.08)	n.a.	98.99
PI-10	7	57.24 (0.67)	26.35 (0.47)	n.a.	0.49 (0.11)	8.45 (0.44)	n.a.	0.32 (0.05)	6.33 (0.37)	n.a.	99.19
PI-11	4	56.77 (0.80)	26.99 (0.47)	n.a.	0.48 (0.06)	8.91 (0.45)	n.a.	0.29 (0.04)	6.01 (0.18)	n.a.	99.45
PI-12	4	58.35 (0.45)	26.31 (0.51)	n.a.	0.50 (0.12)	8.22 (0.33)	n.a.	0.34 (0.09)	6.58 (0.18)	n.a.	100.30
PI-14	5	58.10 (0.67)	26.41 (0.41)	n.a.	0.51 (0.03)	8.27 (0.21)	n.a.	0.34 (0.07)	6.39 (0.14)	n.a.	100.03
PI-15	5	57.39 (0.13)	26.50 (0.35)	n.a.	0.52 (0.08)	8.46 (0.27)	n.a.	0.34 (0.04)	6.31 (0.06)	n.a.	99.51
PI-16	7	58.50 (1.06)	25.14 (0.80)	n.a.	0.48 (0.17)	7.04 (0.75)	n.a.	0.34 (0.07)	7.12 (0.39)	n.a.	98.62
PI-17	4	56.35 (0.48)	26.78 (0.24)	n.a.	0.45 (0.02)	9.13 (0.43)	n.a.	0.27 (0.03)	6.05 (0.16)	n.a.	99.04
PI-20	4	56.99 (1.24)	26.47 (0.37)	n.a.	0.51 (0.06)	8.57 (0.31)	n.a.	0.29 (0.06)	6.20 (0.19)	n.a.	99.02
PI-21	4	60.55 (0.40)	24.00 (0.45)	n.a.	0.24 (0.11)	5.83 (0.33)	n.a.	0.46 (0.05)	7.43 (0.21)	n.a.	98.51
PI-22	7	61.14 (0.55)	24.10 (0.50)	n.a.	0.27 (0.07)	5.76 (0.09)	n.a.	0.43 (0.01)	7.87 (0.09)	n.a.	99.11
PI-24	4	61.25 (0.85)	23.56 (0.62)	n.a.	0.29 (0.10)	5.31 (0.33)	n.a.	0.53 (0.08)	7.79 (0.37)	n.a.	98.73
PI-29	3	60.12 (1.59)	24.15 (1.21)	n.a.	0.50 (0.20)	6.35 (1.26)	n.a.	0.44 (0.07)	7.26 (0.41)	n.a.	98.82
PI-30	1	58.95	25.97	n.a.	0.44	7.73	n.a.	0.38	7.01	n.a.	100.47
PI-31	4	57.27 (0.49)	26.73 (0.53)	n.a.	0.49 (0.05)	8.83 (0.41)	n.a.	0.29 (0.03)	6.34 (0.29)	n.a.	99.95
PI-33	5	59.04 (0.37)	25.55 (0.56)	n.a.	0.38 (0.03)	7.71 (0.30)	n.a.	0.40 (0.07)	7.21 (0.17)	n.a.	100.29
PI-34	6	57.31 (0.35)	26.61 (0.21)	n.a.	0.40 (0.07)	8.78 (0.27)	n.a.	0.30 (0.03)	6.71 (0.07)	n.a.	100.11

The average of *n* analyses (in wt%) is given together with the standard deviation (number in parentheses). Analyses of glass are normalized to 100 wt%, however the non-normalized total is reported.

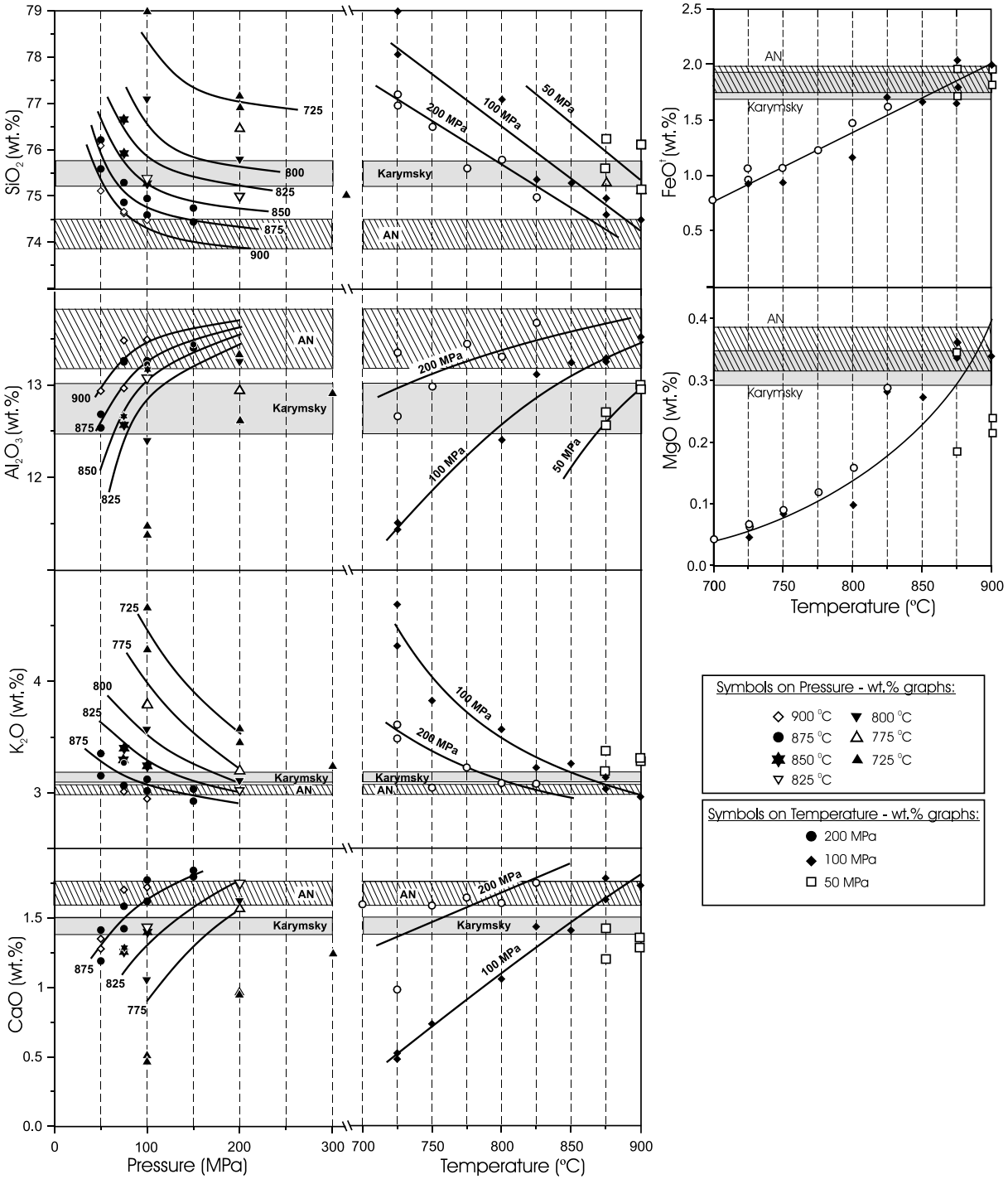

Fig. 5. Variations of experimental melt composition as a function of temperature and pressure. Shaded areas correspond to the average compositions ($\pm 1\sigma$) of matrix glasses in Karymsky and AN dacites.

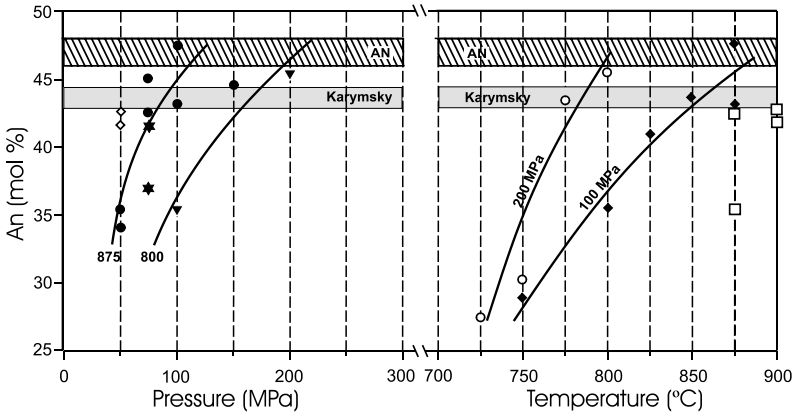

Fig. 6. Variations of experimental plagioclase composition. Shaded areas correspond to average composition (±1σ) of natural plagioclase rims in Karymsky and AN dacites. Symbols are the same as in Fig. 5.

for the origin of compositionally similar dacites of Karymsky and AN caldera-forming eruptions.

6.1. Origin of granophyric xenoliths

Granophyric xenoliths were transported to the surface in 1996 by basaltic magma, which ascended as a dike along a longitudinally oriented fault (Fedotov, 1998; Eichelberger and Izbekov, 2000). Assuming that the dike magma ascended vertically, the granophyres were incorporated directly below the 1996 vent. Because the vent is located within the AN caldera, the source of xenoliths would thus be from a plutonic body situated beneath the caldera. This does not necessarily imply that the pluton is the crystallized remains of the magma chamber that fed the caldera-forming eruption of AN. Indeed, for the last 2 Myr many silicic magmas have erupted at Karymsky volcanic center, and their plutonic remnants may be situated below AN caldera as well (Ivanov, 1970). In addition, granitic plutons compose the Cretaceous metamorphic basement, the upper surface of which is approximately 3–4 km below AN caldera (Balesta, 1991; Sugrobov and Yanovsky, 1991).

We believe, however, that the compositional and textural characteristics of the granophyres clearly indicate that they are genetically linked to the AN dacite, rather than to another source. First, the whole-rock compositions of the granophyres match that of AN dacite (Table 2), whereas no other silicic magma erupted in the area shows such similarity (Masurenkov, 1980). Second, the compositions of plagioclase cores and rare inclusions of clinopyroxenes in the granophyres overlap with those in the AN dacite (Table 3). Finally, the micrographic texture of the groundmass of granophyre is consistent with rapid crystallization caused by significant undercooling, which is likely to occur at a relatively shallow depth, and could be related to a depressurization and volatile loss during the caldera-forming eruption of AN (e.g., Lipman et al., 1997; Lowenstern et al., 1997).

Despite their similar bulk compositions, the mineral assemblage of the granophyric xenoliths differs from that of the AN dacite by the presence of hornblende and biotite, whereas clinopyroxene occurs only as rare inclusions in amphibole phenocrysts. The presence of hornblende+quartz in granophyre allows its crystallization pressure to be inferred using the Al-in-hornblende geobarometer. The concentration of Al_2O_3 in hornblende averages 6.14 ± 0.17 wt% (Table 3), which suggests a crystallization pressure of 100 ± 50 MPa according to the geobarometer of Johnson and Rutherford (1989), calibrated experimentally using similar whole-rock compositions. The algorithm of Anderson and Smith (1995), which takes into account the temperature dependence of Al content in hornblende, yields similar results at temperatures plausible for crystallization of the granophyre: 70 MPa and 135 MPa for 775°C

and 725°C, respectively. Therefore we assume that 100 MPa approximates the crystallization pressure of the granophyre. The inclusions of clinopyroxenes could then be relicts of the reaction of clinopyroxene+melt going to amphibole+biotite, and the overall change from orthopyroxene+clinopyroxene to amphibole+biotite is consistent with isobaric crystallization of the dacite at pressures greater than ~100 MPa (Fig. 4).

Whether granophyre crystallized prior to or after the caldera-forming eruption is uncertain. In either case, it has likely crystallized in the reservoir that produced the caldera-forming eruption of AN, and thus the depth of its crystallization should be approximately the same as the pre-eruptive depth of AN dacite. Therefore, we assume that 100 MPa is a close estimate for the pre-eruptive pressure at which AN dacite was last equilibrated. The solubility of water in rhyolite melt increases with pressure, and equals ~4 wt% at 100 MPa (e.g., Gardner et al., 1999). Glass inclusions in pyroxenes of the AN dacite contain 4.3 ± 0.4 wt% of volatiles, which matches that expected for water solubility at 100 MPa. This correspondence suggests that AN dacite was saturated with water immediately prior to its eruption.

6.2. Pre-eruptive conditions for AN and Karymsky dacites

Equilibrium compositions of minerals and melts in water-saturated magma are controlled by temperature, pressure, and oxygen fugacity. Pre-eruptive temperatures and oxygen fugacities of Karymsky and AN dacites can be estimated using the magnetite–ilmenite geothermometer. Using the mineral formula calculation scheme of Stormer (1983) and the algorithm of Andersen and Lindsley (1988), we estimate that the temperature of AN dacite was 883 ± 19°C at a log f_{O_2} of −10.92 ± 0.12, whereas the temperature of Karymsky dacite was 871 ± 19°C at a log f_{O_2} of −11.26 ± 0.13. The oxygen fugacity of both dacites is approximately one order of magnitude greater than the Ni–NiO buffer curve (NNO+1), which allows us to apply our experimental results to AN and Karymsky magma systems.

These Fe–Ti oxide temperatures and the experimentally determined phase relations indicate that the mineral assemblage of the dacites crystallized at pressures below 125 MPa, because at higher pressures plagioclase becomes unstable (Fig. 4). Pre-eruptive pressures and temperatures of Karymsky and AN dacites can be further con-

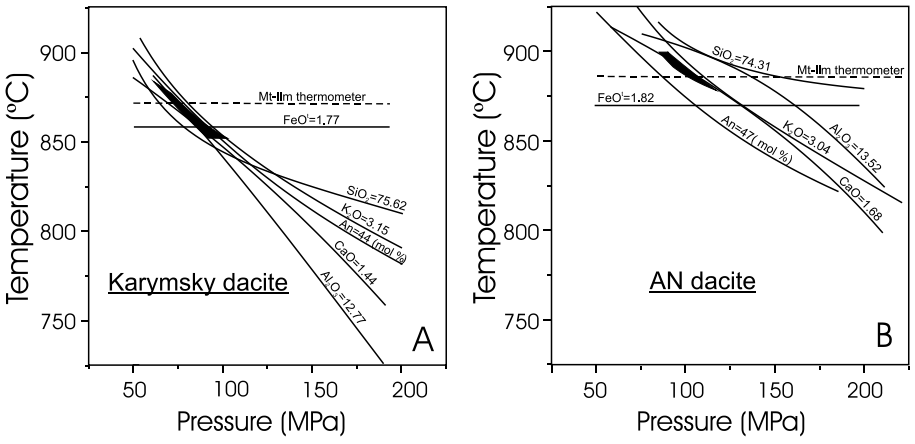

Fig. 7. Isopleths of major oxides in experimental glass and plagioclase compositions (solid lines) that correspond to compositions of matrix glass and plagioclase in Karymsky (A) and AN (B) dacites. Dashed lines show temperatures estimated from natural magnetite–ilmenite pairs in the dacites. Shaded areas correspond to *P–T* conditions where compositions of experimentally produced glass and plagioclase best match those in natural samples.

strained by comparing the compositions of matrix glass in natural samples with those of the experimental runs (e.g., Rutherford et al., 1985; Gardner et al., 1995). In order to determine the most likely pressure–temperature conditions we have defined compositional isopleths as a function of pressure and temperature (Fig. 5). Each isopleth represents a line in pressure–temperature space where the experimental results match the natural compositions of the matrix glasses of the two dacites. Similar compositional isopleths were determined for plagioclase (Fig. 6). The intersection of such isopleths ($\pm\sigma$) for all elements defines a P–T field, in which the compositions of experimental glasses coincide with that of natural samples. Using the glass and plagioclase isopleths in conjunction with the temperatures determined from the natural magnetites and ilmenites constrains the most likely pressure for last equilibrium of the AN dacite to 100 ± 15 MPa. The pressure for last equilibrium of the Karymsky dacite determined in the same way was 85 ± 18 MPa (Fig. 7). We note that the determined pressures match those expected from the average water contents in the glass inclusions.

The inferred pre-eruptive pressures for Karymsky and AN dacites overlap, and correspond to a depth of approximately 3–4 km, assuming a density of 2.6 g/cm^3 for the upper crustal volcanic rocks. This depth coincides with a regional boundary between Cretaceous metamorphic basement and an overlying volcano-sedimentary layer (Balesta, 1991; Sugrobov and Yanovsky, 1991). It is thus possible that the crustal boundary acted as a density window that controlled the emplacement of the dacitic magma bodies below the Karymsky volcanic center.

6.3. Magma system of Karymsky and AN

The similarity of whole-rock compositions, mineral assemblages, and pre-eruptive conditions poses an intriguing question. What kind of magma system could produce compositionally identical magmas, whose eruptions formed similarly sized calderas, yet differ in age by $\sim$30 000 years? The following constraints provide a framework for understanding the magma system at Karymsky and AN: (1) Karymsky and AN calderas have similar sizes, and are centered $\sim$9 km apart. (2) The whole-rock compositions of dacites are the same. (3) Karymsky dacite erupted $\sim$30 000 years after the AN dacite. (4) Pre-eruptive temperatures of Karymsky and AN dacites were 871 ± 19°C and 883 ± 19°C, respectively. (5) Karymsky and AN dacites were last equilibrated approximately at the same depth of ca. 3–4 km. (6) Volcanic activity at Karymsky resumed with basalts only 2500 years after the caldera-forming eruption, which suggests that the remnants of the Karymsky dacitic reservoir were already solidified.

One way to resolve all of the constraints is that caldera-forming events at Karymsky and AN resulted from two separate episodes of partial melting of the lower crust, subsequent ascent, and eruption of separate dacitic batches at 40 000 yr BP and 7900 yr BP (Fig. 8A). Repeated production of compositionally similar magmas is possible if the composition of a crustal substrate was not modified by previous withdrawals, and/or if the composition of produced melt was strictly constrained by a limited number of factors. These factors may include, for example, the critical porosity of a partially molten substrate at which melt is able to segregate to larger volumes and then to ascend.

The close location of the calderas, however, suggests that both Karymsky and AN dacites originated from the same crustal domain or, if separate, from two closely located crustal domains. Even if it were possible to generate large volumes of dacitic magma in a period of time as short as 30 000 years, it would still be very unlikely that the composition of the parental substrate would not be modified by previous melting episodes and the trace element composition of the produced melts would remain exactly the same.

Alternatively both dacites could have been generated at the same time and, at least temporarily, shared the same magma reservoir. Because Karymsky and AN dacites were last equilibrated at the same pressure (3–4 km depth), they could have erupted from the same longitudinally elongated magma body (Fig. 8B), which intruded to that level approximately 40 000 years ago (Ivanov, 1970).

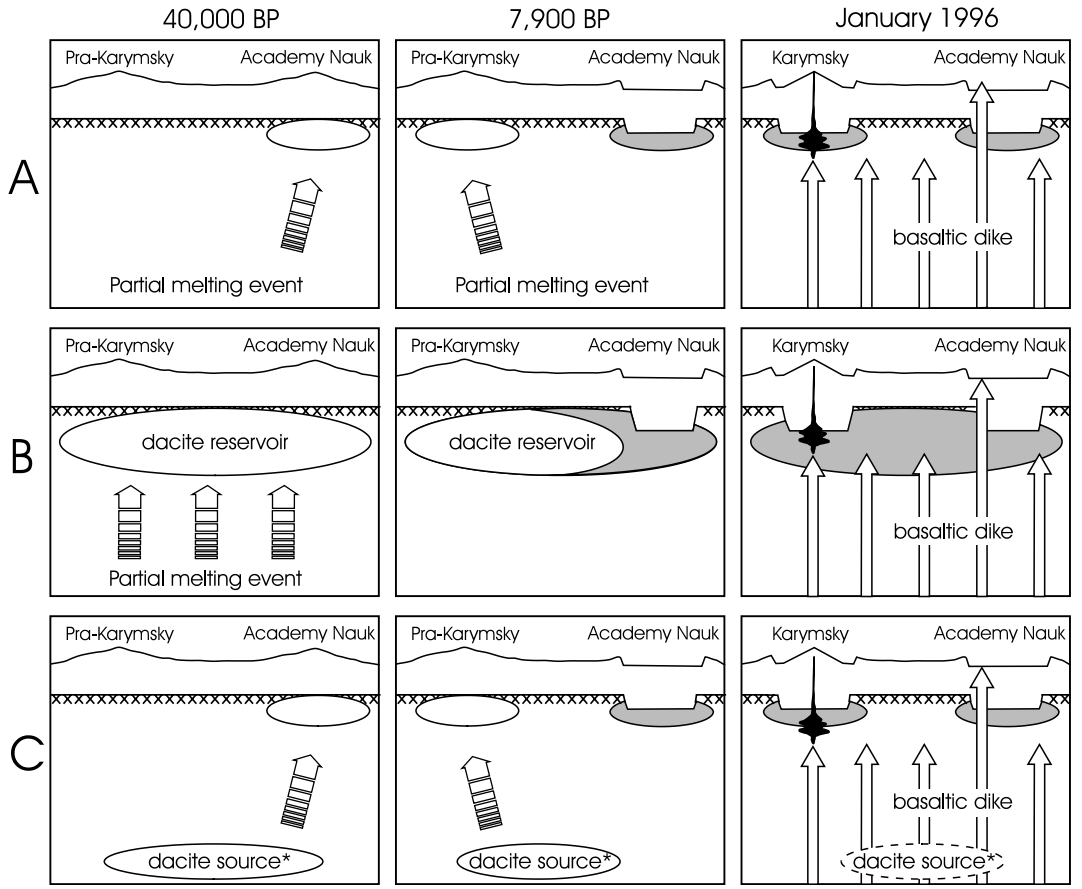

Fig. 8. Possible scenarios for the sequence of caldera-forming events at Karymsky and AN (see text for discussion). (A) Separate partial melting events produce small batches of dacite (10–12 km^3), which ascend and cause the caldera-forming eruptions at 40 000 yr BP and 7900 yr BP. (B) Large dacitic body ($\sim$200 km^3) ascends and feeds the caldera-forming eruptions at 40 000 yr BP and 7900 yr BP. (C) Two separate 10–12-km^3 batches of dacite are derived from a single magma reservoir situated in the lower crust. In all scenarios a basaltic dike in January 1996 samples the crystallized dacitic reservoir, which produced the AN caldera-forming eruption. Gray area represents crystallized dacite. Black area represents the andesitic reservoir of Karymsky stratovolcano. The shaded horizontal line represents a regional boundary between Cretaceous metamorphic basement and an overlying volcano-sedimentary layer at 3–4 km depth (Balesta, 1991; Sugrobov and Yanovsky, 1991). *Either a dacite reservoir produced by previous partial melting, or, alternatively, a large, long-lived mafic zone with extractable interstitial dacitic melt.

Thermal balance considerations in conjunction with outlined earlier constraints can help to evaluate this scenario. Numerical modeling of the thermal regime using the HEAT algorithm (Wohletz et al., 1999) requires the minimum volume of the reservoir to have been $\sim$200 km^3 in order for it to cool from 885°C to 870°C in $\sim$30 000 years. The total volume of dacite erupted 7900 yr BP at Karymsky is 5–7 km^3 (Braitseva and Melekestsev, 1991), and so there should be more than 190 km^3 of magma remaining in the reservoir. The eruption of basalts 2500 years after the formation of Karymsky caldera suggests to us that the portion of reservoir beneath the caldera had already solidified, otherwise the dacitic magma would either trap the intruding basalt or be erupted together with the basalt. It seems unlikely that 190 km^3 of magma could solidify so rapidly, given that it was cooling so slowly before the eruption. Indeed, our modeling suggests a magma body greater than 5 km^3 would still be molten after 2500 years, even assuming efficient heat loss through a highly

conductive/convective layer of cauldron material. In addition, it seems unlikely that a single elongated reservoir would form two separate circular-shaped calderas, instead of one.

We believe the identical compositions of Karymsky and AN dacite require that both derived from the same magma source, which did not evolve compositionally and did not cool significantly in 30 000 years. In contrast, a relatively fast solidification of the remnants of the Karymsky dacite reservoir requires that its pre-eruptive volume would not exceed 10–12 km^3, which would be equivalent to the total of magma erupted (5–7 km^3) plus a maximum volume of magma remained (5 km^3).

One hypothesis, which may reconcile these constraints, is that two separate 10–12-km^3 batches of dacite were derived from a single source situated in the lower crust (Fig. 8C). At 40 000 yr BP, the first portion of dacite detached from the parental body, ascended along the active fault zone until it reached the structural boundary at 3 km, re-equilibrated to that shallow depth, and then erupted. At 7900 yr BP, a second portion of dacite, perhaps representing much of the melt remaining in the parental body, ascended along the same fault zone until reaching the 3-km boundary, re-equilibrated, and erupted. The amount of time required for the dacites to re-equilibrate is not known, but would need to be long enough to erase any vestige of a high-pressure mineral assemblage. For example, hornblende would be stable in the magmas at water pressures greater than 200 MPa, and it would have to completely break down in the 100-MPa storage zone.

The lower crustal source region could be a relatively mafic zone – of either old crust or arc plutonic material or both – containing interstitial dacitic melt with a distributed melt volume and melt life span much greater than that of an individual caldera cycle. Caldera-forming melt batches could then repeatedly escape, changing the source region very little. The source region would need to contain a high enough melt fraction to be permeable to melt flow, but a low enough melt fraction to behave as a solid and fracture as basalts such as the 1996 basalt intruded and passed through it.

7. Conclusions

(1) Granophyre xenoliths were sampled by ascending basalt from a crystallized silicic reservoir, which produced the caldera-forming eruption of AN 40 000 yr BP. According to Al-in-hornblende geobarometry, this granophyre crystallized at a depth corresponding to 100 MPa.

(2) Compositions of Fe–Ti oxides, H_2O contents of glass inclusions, and results of phase-equilibrium experiments suggest that AN and Karymsky dacites were last equilibrated at water-saturated conditions and an oxygen fugacity of NNO+1. Immediately prior to eruption, AN dacite was stored at 883 ± 19°C and situated at a depth corresponding to a pressure of 100 ± 15 MPa. Pre-eruptive conditions for the 7900 yr BP Karymsky dacite were 871 ± 19°C and 85 ± 18 MPa.

(3) Similar whole-rock compositions of AN and Karymsky dacites suggest that they were derived from the same dacite-bearing crustal source, which did not evolve compositionally between the two caldera-forming eruptions. Most likely, a small ($\sim$10-km^3) batch of the dacite detached from the parental reservoir, ascended to a stratigraphic boundary at 3 km depth, and erupted at 40 000 yr BP. This process was repeated at 7900 yr BP.

Acknowledgements

This work was supported by the Volcano Hazards Program of the U.S. Geological Survey through the Alaska Volcano Observatory. Help of Jessica Larsen and Jacob Lowenstern in acquiring the FTIR data is highly appreciated. Thorough and constructive reviews of Malcolm Rutherford, Michael Dungan, and Bruce Marsh are gratefully acknowledged.

References

Anders, E., Grevesse, N., 1989. Abundances of the elements: meteoric and solar. Geochim. Cosmochim. Acta 53, 197–214.

Andersen, D.J., Lindsley, D.H., 1988. Internally consistent solution models for Fe-Mg-Mn-Ti oxides: Fe-Ti oxides. Am. Mineral. 73, 714–726.

Anderson, J.L., Smith, D.R., 1995. The effects of temperature and f_{O2} on the Al-in-hornblende barometer. Am. Mineral. 80, 549–559.

Bacon, C.R., Hirschmann, M.M., 1988. Mg/Mn partitioning as a test for equilibrium between coexisting Fe-Ti oxides. Am. Mineral. 73, 57–61.

Balesta, S.T., 1991. Earth crust structure and magma chambers of the areas of present Kamchatka volcanism. In: Fedotov, S.A., Masurenkov, Y.P. (Eds.), Active Volcanoes of Kamchatka. Nauka, Moscow, pp. 36–45.

Belousov, A., Belousova, M., 2001. Eruptive process, effects and deposits of the 1996 and ancient basaltic phreatomagmatic eruptions in Karymskoye lake, Kamchatka, Russia. Spec. Publ. Int. Assoc. Sedimentol. 30, 35–60.

Braitseva, O.A., 1998. Phreatomagmatic eruption in Lake Karymskoe (East Kamchatka) ~6500 ^{14}C years BP and Holocene episodes of basalt magma injection under the Karymsky area. Volcanol. Seismol. 19, 685–692.

Braitseva, O.A., Melekestsev, I.V., 1991. Eruptive history of Karymsky Volcano, Kamchatka, USSR, based on tephra stratigraphy and ^{14}C dating. Bull. Volcanol. 53, 195–206.

Devine, J.D., Gardner, J.E., Brack, H.P., Layne, G.D., Rutherford, M.J., 1995. Comparison of microanalytical methods for estimating H_2O contents of silicic volcanic glasses. Am. Mineral. 80, 319–328.

Eichelberger, J.C., Izbekov, P.E., 2000. Eruption of andesite triggered by dyke injection; contrasting cases at Karymsky Volcano, Kamchatka and Mt Katmai, Alaska. Phil. Trans. R. Soc. Math. Phys. Eng. Sci. 358, 1465–1485.

Fedotov, S.A., 1998. Study and mechanism of the simultaneous 1996 Karymsky volcano and Academy Nauk caldera eruptions in Kamchatka. Volcanol. Seismol. 19, 521–524.

Gardner, J.E., Rutherford, M., Carey, S., Sigurdsson, H., 1995. Experimental constraints on pre-eruptive water contents and changing magma storage prior to explosive eruptions of Mount St Helens Volcano. Bull. Volcanol. 57, 1–17.

Gardner, J.E., Hilton, M., Carroll, M.R., 1999. Experimental constraints on degassing of magma; isothermal bubble growth during continuous decompression from high pressure. Earth Planet. Sci. Lett. 168, 201–218.

Gardner, J.E., Layer, P.W., Rutherford, M.J., 2002. Phenocrysts versus xenocrysts in the youngest Toba Tuff: Implications for the petrogenesis of 2800 km^3 of magma. Geology 30, 347–350.

Geschwind, C.-H., Rutherford, M.J., 1992. Cummingtonite and the evolution of the Mount St. Helens (Washington) magma system: an experimental study. Geology 20, 1011–1014.

Grib, E.N., 1998. Petrology of ejecta produced by the Akademii Nauk caldera eruption of January 2–3, 1996. Volcanol. Seismol. 19, 605–636.

Huppert, H.E., Sparks, R.S.J., 1988. The generation of granitic magmas by intrusion of basalt into continental crust. J. Petrol. 29, 599–624.

Ivanov, B.V., 1970. Eruption of Karymsky Volcano during 1962–65 and the Karymsky Volcanic Group. Nauka, Moscow, 135 pp. (in Russian).

Izbekov, P.E., Eichelberger, J.C., Patino, L.C., Vogel, T.A., Ivanov, B.V., 2002. Calcic cores of plagioclase phenocrysts in andesite from Karymsky volcano: Evidence for rapid introduction by basaltic replenishment. Geology 30, 799-802.

Johnson, M.C., Rutherford, M.J., 1989. Experimentally determined conditions in the Fish Canyon Tuff, Colorado, magma chamber. J. Petrol. 30, 711–737.

Lipman, P.W., 1967. Mineral and chemical variations within an ash-flow sheet from Aso Caldera, southwestern Japan. Contrib. Mineral. Petrol. 16, 300–327.

Lipman, P.W., Dungan, M.A., Bachmann, O., 1997. Comagmatic granophyric granite in the Fish Canyon Tuff, Colorado; implications for magma-chamber processes during a large ash-flow eruption. Geology 25, 915–918.

Lowenstern, J.B., Clynne, M.A., Bullen, T.D., 1997. Comagmatic A-type granophyre and rhyolite from the Alid volcanic center, Eritrea, Northeast Africa. J. Petrol. 38, 1707–1721.

Masurenkov, Y.P., 1980. Volcanic Centers: Formation, Dynamics, Properties (Karymsky Structure). Nauka, Moscow, 300 pp. (in Russian).

Nye, C.J., Swanson, S.E., Avery, V.F., Miller, T.P., 1994. Geochemistry of the 1989–1990 eruption of Redoubt Volcano; Part I, Whole-rock major- and trace-element chemistry. J. Volcanol. Geotherm. Res. 62, 429–452.

Rutherford, M.J., Sigurdsson, H., Carey, S., Davis, A., 1985. The May 18, 1980, eruption of Mount St. Helens; 1, Melt composition and experimental phase equilibria. J. Geophys. Res. B 90, 2929–2947.

Sparks, R.S.J., Huppert, H.E., Wilson, C.J.N., Halliday, A.N., Mahood, G.A., 1990. Evidence for long residence times of rhyolitic magma in the Long Valley magmatic system; the isotopic record in precaldera lavas of Glass Mountain; discussion and replies. Earth Planet. Sci. Lett. 99, 387–399.

Stormer, J.C., Jr., 1983. The effects of recalculation on estimates of temperature and oxygen fugacity from analyses of multicomponent iron-titanium oxides. Am. Mineral. 68, 586–594.

Sugrobov, V.M., Yanovsky, F.A., 1991. Geothermal field of Kamchatka, heatlosses by volcanoes and hydrotherms. In: Fedotov, S.A., Masurenkov, Y.P. (Eds.), Active Volcanoes of Kamchatka. Nauka, Moscow, pp. 58–71.

Sutton, A.N., Blake, S., Wilson, C.J.N., 1995. An outline geochemistry of rhyolite eruptives from Taupo volcanic centre, New Zealand. J. Volcanol. Geotherm. Res. 68, 153–175.

Volynets, O.N., Ponomareva, V.V., Braitseva, O.A., Melekestsev, I.V., Chen, C.H., 1999. Holocene eruptive history of Ksudach volcanic massif, South Kamchatka; evolution of a large magmatic chamber. J. Volcanol. Geotherm. Res. 91, 23–42.

Wohletz, K., Civetta, L., Orsi, G., 1999. Thermal evolution of the Phlegraean magmatic system. J. Volcanol. Geotherm. Res. 91, 381–414.